nature photonics

Article

https://doi.org/10.1038/s41566-024-01483-2

All-optical temporal logic gates in localized exciton polaritons

Received: 1 September 2023

Accepted: 17 June 2024

Published online: 2 August 2024

Check for updates

Hui Li[1,7] ✉, Fei Chen[1,2,7], Haoyuan Jia[1,7], Ziyu Ye[1], Hang Zhou[3], Song Luo[3], Junheng Shi[4], Zhenrong Sun[1], Huailiang Xu[1], Hongxing Xu[1], Tim Byrnes[1,5], Zhanghai Chen[3] & Jian Wu[1,6] ✉

Exciton polaritons—quasi-particle excitations consisting of strongly coupled photons and excitons—present fascinating possibilities for photonic circuits, owing to their strong nonlinearity, ultrafast reaction times and their ability to form macroscopic quantum states at room temperature via non-equilibrium condensation. Past implementations of transistors and logic gates with exciton polaritons have been mostly realized using the spatial propagation of polariton fluids, which place high demands on the fabrication of the microcavities and typically require complex manipulations. In this work we have implemented the full set of logical gate functionalities (that is, temporal AND, OR and NOT gates) in localized exciton polaritons at room temperature, on the basis of precisely controlling the interplay between polariton condensate and exciton reservoir dynamics, using a two-pulse excitation scheme. The dynamics intrinsically covers the cascadability required by the logical operations, enabling efficient information processing without the need for spatial flow. The temporal polariton logic gates demonstrate advantages in ultrafast switching, universality and simplified compatibility with other dimensional controls, showing great potential for building polariton logic networks in strongly coupled light–matter systems.

Improving the performance of information encoding and processing is an ongoing objective for optical integrated circuits. Practical multiplexing schemes have been developed in the field of optical information science and technology[1], where dimensions such as time[2,3], space[4], wavelength[5], polarization[6] and angular momentum[7,8] are effectively used to increase the processing rate and capacity. Although photons as information carriers have the advantage of fast response times, low energy consumption and negligible heating[9], their weak inter-particle interactions place demands on the ability to modulate them. One way of avoiding this bottleneck is to use the quantum systems formed by strong light–matter coupling. Remarkable developments in material science and microcavity fabrication techniques have made it possible to confine photons to extremely small mode volumes and achieve strong coupling between cavity photons and semiconductor excitons, yielding hybrid bosonic quasiparticles called exciton polaritons (EPs)[10,11].

Exciton polaritons inherit the advantages of a light effective mass and fast propagation speed from their photonic component, and strong nonlinearity from their excitonic constituents[12]. They are capable of achieving bosonic condensation at high temperatures[13–15], and the resulting non-equilibrium macroscopic quantum state presents

[1]State Key Laboratory of Precision Spectroscopy, East China Normal University, Shanghai, China. [2]Peking University Yangtze Delta Institute of Optoelectronics, Nantong, China. [3]Department of Physics, College of Physical Science and Technology, Xiamen University, Xiamen, China. [4]CAS Key Laboratory of Theoretical Physics and Institute of Theoretical Physics, Chinese Academy of Sciences, Beijing, China. [5]New York University Shanghai, NYU-ECNU Institute of Physics at NYU Shanghai, Shanghai Frontiers Science Center of Artificial Intelligence and Deep Learning, Shanghai, China. [6]Collaborative Innovation Center of Extreme Optics, Shanxi University, Taiyuan, China. [7]These authors contributed equally: Hui Li, Fei Chen, Haoyuan Jia. ✉e-mail: hli@lps.ecnu.edu.cn; jwu@phy.ecnu.edu.cn

fascinating possibilities for information processing[16,17]. Device functionalities such as polaritonic lasers[18,19], switches[20–23], routers[24,25], transistors[20,26,27] and logic gates[26,28,29] have been demonstrated in EP systems, some of which can even operate at room temperature. Nevertheless, most of the functional operations—especially at ambient conditions—are based on manipulating the quasiparticles in the spatial domain[26,27], or in the combination of temporal and spatial domains[29]. The spatially dependent control relies heavily on the properties of the microcavity, thus placing higher demand on the microcavity design and preparation. An alternative to such approaches is to exploit the temporal degree of freedom, which can be used to perform and process information without interference in the other dimensions; however, functional control of EPs in a purely temporal dimension is hitherto largely absent, especially at room temperature. A detailed understanding of the dynamical properties is crucial to realizing temporal domain manipulation; however, this has been hindered to some extent by a lack of development of techniques that involve high-precision, time-resolved multidimensional measurements.

In this work we provide reliable schemes for the realization of the full set of polariton temporal logical gates (that is, AND, OR and NOT gates) in a localized EP ensemble, on the basis of precisely controlling the interplay dynamics between the exciton reservoir and the polariton condensates, using a two-pulse excitation scheme. The temporal degree of freedom is a powerful dimension for manipulating information, and is intrinsically uncorrelated with other dimensions. The task of multichannel processing of information can therefore be achieved more easily, and with increasing speed and capacity. The challenge lies in controlling the interactions between the exciton reservoir and the polariton condensates, and directly measuring the temporal modes of the EP quantum states. Control of the macroscopic quantum state can be implemented by taking advantage of techniques generating non-equilibrium hybrid quasi-particle ensembles and accurately measuring the complex temporal waveform with femtosecond resolution. As we show in this work, the dynamical response of the localized EP ensemble in a one-dimensional (1D) ZnO whispering gallery microcavity can be manipulated using non-resonant multiple femtosecond laser pulse injections. By precisely tuning the strength and the relative time delay of the two excitation laser pulses, temporal AND, OR and NOT logical gates have been demonstrated in the subpicosecond to picosecond regime (Fig. 1). Two successive input pulses, denoted input A and input B, are normally sent into a ZnO microcavity at the same location, where their incident strength and relative delay are well-controlled. The leaking photoluminescence emission originating from the EPs in the transmission direction acts as the 'output'. The cascadability, which is crucial for the AND and OR logical operations, can be intrinsically satisfied in the stimulated amplification dynamics in the localized EP ensemble, thereby removing the need of multiple-location injection and controlling the spatial flowing EPs. The NOT gate is realized on the basis of control of the bosonic cascading dynamics of EPs in the multimode ZnO microcavity. The behaviour of the time-resolved photoluminescence emission meets the criteria of the full set of logical gates.

Polariton temporal NOT gate based on EP cascading modes

Realization of the NOT gate is the last missing piece to accomplishing a full set of logical gates in EPs. A step further from past demonstrations in polariton systems, which aimed to switch off an existing signal when providing an electrical[30] or optical[20–23] control, the basic criteria of a polariton NOT gate is to switch off the signal when the control arrives, accompanied by a signal recovery when the control is ended. It requires a more precise and complex manipulation on the underlying dynamics. ZnO microcavities possess multimode spectra that are associated with whispering gallery modes; these multimode spectra allow for bosonic cascading relaxation of EPs[31,32], providing a promising platform for demonstrating a polariton NOT gate. In our experiment, EPs are formed in a 1D ZnO microcavity by non-resonant pumping using femtosecond laser pulses at a central wavelength of 350 nm, at which there is strong coupling between the cavity photons and electron–hole pairs[33]. The dispersion relation of the EPs can be obtained by probing the angle-resolved spectra of the Fourier-plane photoluminescence emission using a spectrometer implemented with a two-dimensional detector, where the angle represents the in-plane momentum of the polariton wavepacket. As the pumping fluence is increased beyond a certain threshold ($F_{th} \approx 1.2$ mJ cm^{-2}), polariton condensates (Fig. 2a inset) form in the ground states of two lower polariton branches, denoted by modes U and L, respectively. It has been shown that there is a ladder of discrete energy levels in the 1D ZnO microcavity, which sustain the bosonic cascading process for EPs, that is, stimulated transition between neighbouring energy levels[34]. In this work, EP condensates are initially induced using non-resonant excitation by a beam of femtosecond pulses, producing the 'on' state at mode U, indicated by the inset angle-resolved spectra in Fig. 2a. Another beam of control pulses arriving at a proper time delay interacts with the EP condensate and depletes the population of mode U via cascading relaxation, resulting in a population increase on the neighbouring mode L (as shown in the inset marked 'off' in Fig. 2a). The pumping and the control fluences are about $1.2F_{th}$ and $0.1F_{th}$, respectively. In Fig. 2a, the spectra of the EP condensates are shown as a function of the relative time delay between the pump and the control pulses. A polariton NOT gate with a close to zero time delay between the two pulses can be achieved, where a clear 'switching off' behaviour can be found for mode U, with a corresponding increase of the signal on mode L. The control pulse acts as the input, whereas the leaking photoluminescence emission of mode U serves as the output. When the input is off, the polariton condensate at mode U is on, while the polariton signal can be switched off at the arrival of the control pulse, corresponding to a 1–0 operation. The full-width at half-maximum (FWHM) of the temporal response to switching from on to off is ~80 fs; this was extracted from the output signal of mode U as a function of the delay time (Fig. 2b). The dynamics can be well-reproduced by modelling using rate equations, demonstrating the dominance of the enhanced cascading relaxation in EPs when the pump and the control pulses overlap[34]. This ultrafast response time is one order of magnitude shorter than the recently reported subpicosecond response time of the polariton switch[29]. The switching energy obtained from the control pulse is at the level of several tens of picojoules per operation, and a ~15 dB On and Off contrast can be obtained. Compared with various optical switches, this polariton NOT gate exhibits advantages of ultrafast switching time and high contrast[35].

As the time delay approaches zero, dramatic interactions take place in the polariton system. The underlying dynamics of the NOT gate can be revealed using the femtosecond angle-resolved spectroscopic imaging (FARSI) technique[36]. As presented in Fig. 2c,d, the dynamics for the 'on' and 'off' states of the logic NOT gate are obtained at fixed time delays of 200 fs and 0 fs, respectively. The real buildup time for the EP condensates can be extracted to be on picosecond timescales (~9.6 ps for the 'on' state). Close to the zero time delay, the co-excitation of the pump and the control pulses induce a larger local population, therefore accelerating the underlying buildup and relaxation dynamics of EPs[37]. An energy blue-shift of up to about 9 and 20 meV is observed for the U and the L modes, respectively, at close to zero time delay, which can be attributed to the enhanced inter-particle interactions at a higher local density. The actual buildup speed of the EP condensate is dominated by the total injection, thus the 'off' state operated close to zero time delay experiences a faster dynamical process.

Polariton temporal AND gate by non-resonant injections

When the pumping fluence is slightly beyond the condensation threshold F_{th}, a polariton condensate forms in the ground state of the lower

https://doi.org/10.1038/s41566-024-01483-2

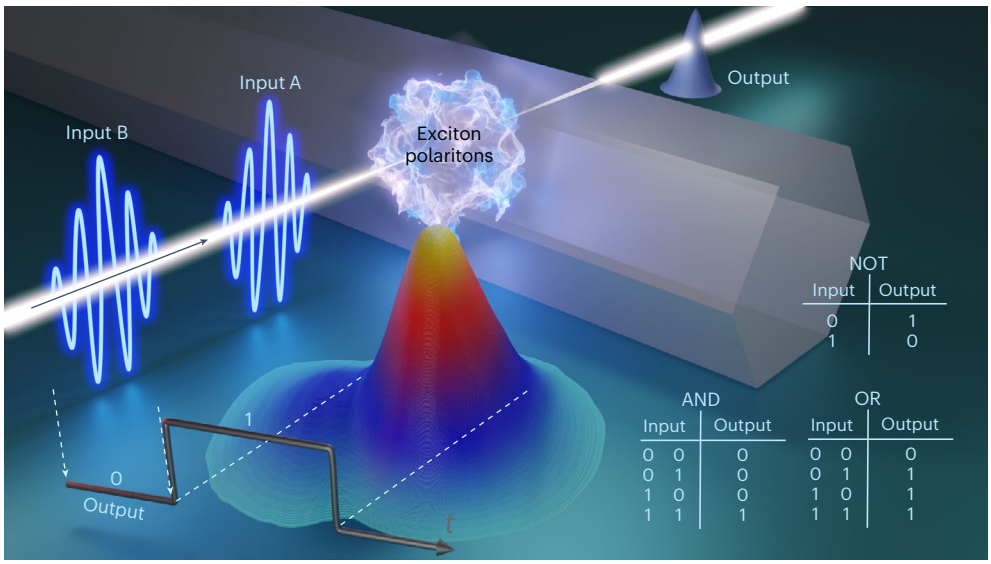

Fig. 1 | Polaritonic temporal logic gates. Two femtosecond laser pulses, denoted input A and input B, are incident at the same point on a ZnO microcavity to manipulate the underlying dynamics of the macroscopic quantum states. The leaking photons can be detected as the 'output' signal in the transmission direction. The full set of logical gate functions are realized in the localized EP ensemble. The polariton NOT gate is realized on the basis of tailored bosonic cascading relaxation of several polariton modes in a ZnO microcavity. The arrival of the control pulse can shut off an existing polariton Bose–Einstein condensate (BEC) by driving the polariton population to the neighbouring polariton branch. The AND and OR logical gates are created through stimulated amplification, which is driven by two pumping laser pulses. The behaviour of the time-resolved photoluminescence emission (illustrated by the coloured profile) meets the criteria of the full set of logical gates shown in the tables, depending on the specific injection levels and time delays between the two pumping pulses.

polariton branch. In this case, a clear blue-shift and a sharp reduction in the momentum distribution is observed (as shown in Fig. 3b), demonstrating condensate formation[38]. The buildup dynamics of the polariton condensate for this specific geometry has been reported recently under the non-resonant excitation condition[37], where the initially excited hot excitons take multiple steps to relax towards the ground state, resulting in EP condensation within a few picoseconds. Although EPs have a lifetime in the region of picoseconds, the excited exciton reservoir possesses a much longer lifetime at the subnanosecond to nanosecond timescales[39]. This provides us a platform to manipulate the dynamical response of the polariton ensemble.

Interestingly, when the pumping strength of a single driving laser pulse is insufficient to produce condensation, two successive equal injections (bi-injections) can realize condensation through stimulated amplification. Furthermore, the condensate population can be controlled by a subsequent injection, where the relative time delay between the two pumping pulses is precisely controlled. Here, by using bi-injections at a pumping strength of $F \approx 0.6F_{th}$, condensation occurs as long as the relative time delay between the two injection pulses is shorter than about 120 ps (Fig. 3d). The static-state angle-resolved spectra obtained for this bi-injection (shown in Fig. 3c) is similar to what is obtained under single-pulse injection. The difference in the dynamics can be explicitly visualized using the FARSI technique. The condensation signal monotonically decreases with larger relative time delays between the two injection pulses (shown in Fig. 3e), accompanied by an increase in the linewidth and in the buildup time (Fig. 3f).

The underlying process can be revealed on the basis of a theoretical model using the Gross–Pitaevskii equation coupled to an incoherent exciton reservoir[37]. The simulation results are shown in Fig. 3g. The injection of the first laser pulse will generate a dynamical exciton reservoir density, n_R, with a long decay time. An instantaneous stimulated amplification can be induced by the second laser pulse when a 'seed' population exists in the localized exciton ensemble. The gain can be over one order of magnitude (depending on the injection time and strength of the second pulse) so that the critical density for condensation can be achieved through bi-injections. Although the gain of the exciton population builds up quickly at subpicosecond timescales, the system requires more time to buildup a polariton condensate. The final output can be delayed by more than 10 ps with respect to the arrival time of the second laser pulse, agreeing with the observations shown in Fig. 3e. Delay-dependent reduction

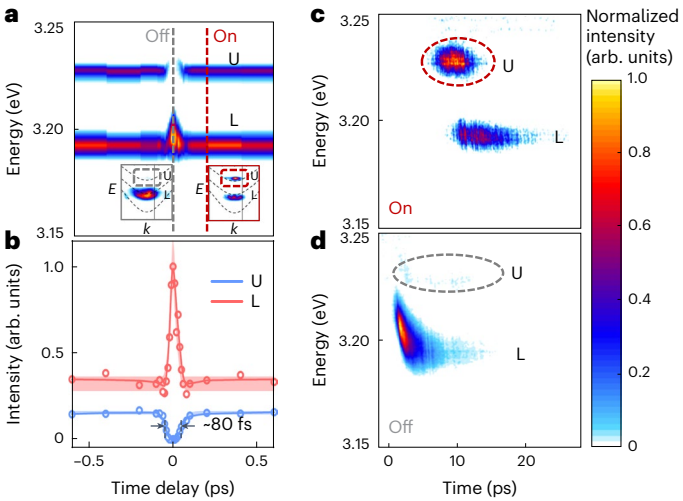

Fig. 2 | Polariton temporal NOT gate based on manipulating the bosonic cascading relaxation in exciton polaritons. The NOT gate is obtained by using two-pulse non-resonant injection, with the pump and control pulses fixed at ~$1.2F_{th}$ and $0.1F_{th}$, respectively. **a**, Photoluminescence emission spectra of EPs as a function of the time delay between the pump and the probe pulses. The insets show time-integrated dispersion of the photoluminescence distributions at time delays of 200 fs and 0 fs, which correspond to the 'on' and 'off' states for the output signal, respectively. E is the energy and k is the in-plane momentum. **b**, Integrated signal intensity for the U and the L polariton modes as a function of the time delay. The scattered data are obtained from experiments. The solid curves are calculation results obtained on the basis of rate equations involving the cascading process between the polariton modes[34]. Data are presented as mean values with 95% CI ($n = 3$). The blue curve represents a NOT gate function close to zero time delay. A ~80 fs FWHM of the response time is obtained. **c**,**d**, Time-resolved spectra of the photoluminescence emission as a function of time for the 'on' (**c**) and 'off' (**d**) output states. The time delays are at 200 fs and 0 fs, respectively.

https://doi.org/10.1038/s41566-024-01483-2

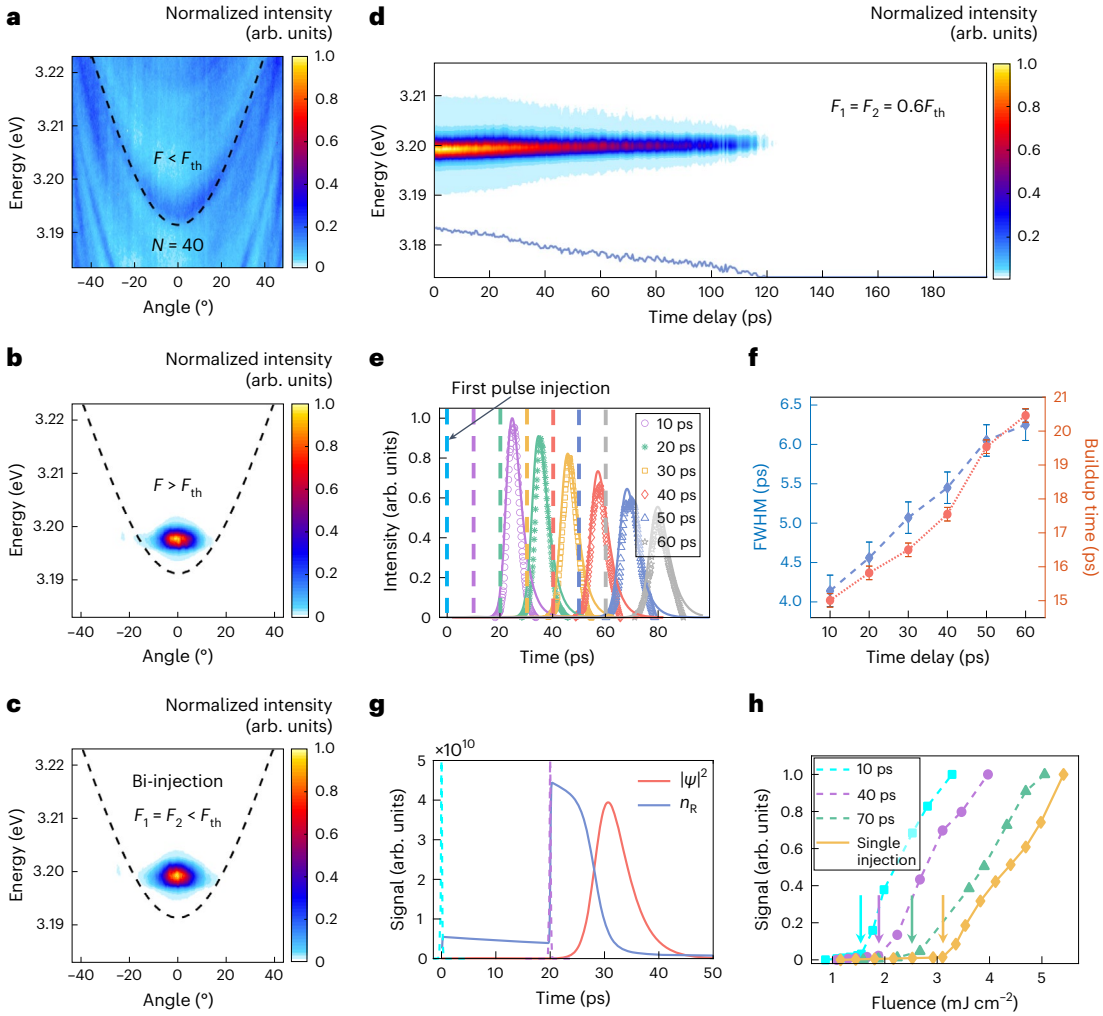

Fig. 3 | Localized exciton polaritons excited by multiple non-resonant injections. a–**c**, The integrated angle-resolved spectra for single-pulse injection below (**a**) and above (**b**) the condensation threshold, and for two successive pulse injections (**c**) at a delay of 5 ps. The fluence of each pulse is kept at about $0.6F_{th}$. **d**, Spectra for two pulse injections as a function of the time delay. Condensation can be achieved within a delay of about 120 ps. **e**, Time-resolved photoluminescence intensity obtained for the indicated relative delays. The light blue dashed line represents the arrival of the first excitation pulse at zero time delay. The dashed lines of other colours indicate the arrival time of the second excitation laser pulses. **f**, The linewidth and buildup time of the resulting condensation signals for bi-injection at various delays. Error bars are estimated from the experimental instability ($n = 3$). **g**, Simulation results based on solving the open-dissipative GP equation. The light blue dashed line indicates the injection of the first laser pulse at zero time delay. The dark blue curve shows the dynamics of exciton density where the sudden enhancement at about 20 ps is induced by the second pulse injection (marked by the purple dashed line). The red curve represents the time-resolved EP population produced by stimulated amplification. $|\psi|^2$ is the density of the lower polariton mode, which is presented by a magnification of 70 times for better comparison. n_R represents the calculated density of the exciton reservior. **h**, Threshold behaviours as a function of the second injection fluence with delays of 10, 40 and 70 ps, respectively. The dark yellow curve represents a single-pulse injection scenario.

of the gain is well-reproduced in this model (refer to the solid curves in Fig. 3e). The degree of enhancement is mainly determined by the instantaneous quantity of the exciton density and the strength of the second laser pulse. The shorter the time delay, the higher the instantaneous n_R, and hence the condensation threshold (for the second pulse) can be reduced for shorter delays (as shown in Fig. 3h). Comparison of the condensation threshold has been made for various second pulse injection instants (that is, at 10 ps, 40 ps and 70 ps) with respect to the single beam injection case (Fig. 3h). The fluence dependence shows that the condensation threshold can be reduced by approximately 50% when the second pulse arrives at a time delay of 10 ps, compared with that for the single-injection case. The threshold reduction is stronger for shorter time delays.

A two-stage injection method can achieve AND logic gate operation by dynamically amplifying a localized polariton ensemble. The output of the first stage can act as the input of the second stage without physical propagation, which removes the necessity of manipulating the polariton flow spatially. As sketched in Fig. 1, a temporal AND gate can be achieved when the input signals for A and B are both below the condensation threshold (that is, $F_A < F_{th}$ and $F_B < F_{th}$) and their sum is beyond the threshold ($F_A + F_B > F_{th}$). The discrimination level for both the input and the output signals should be around 0, such that 0 represents no signal. If polaritonic condensation cannot be established by the injections, the output will be '0'. The inserted profile is obtained from a real measurement and the corresponding discriminated signal represent an output at '1'. In this geometry, two input signals at '0', or either input as '1', can produce an output at '0'. Only when both the inputs are 1 will the output be 1. The relative delay between the two injection pulses need to be controlled to be a certain time delay within, for example, 120 ps, for the specific case presented in Fig. 3. The amplification gain is determined by the different injection levels and times, with sufficient extinction ratio for real-life operation. This scheme based on the temporal domain operation of EPs can be universally applied to various semiconductor microcavities, dramatically reducing the requirement for cavity uniformity which is crucial for flow-dependent manipulation.

https://doi.org/10.1038/s41566-024-01483-2

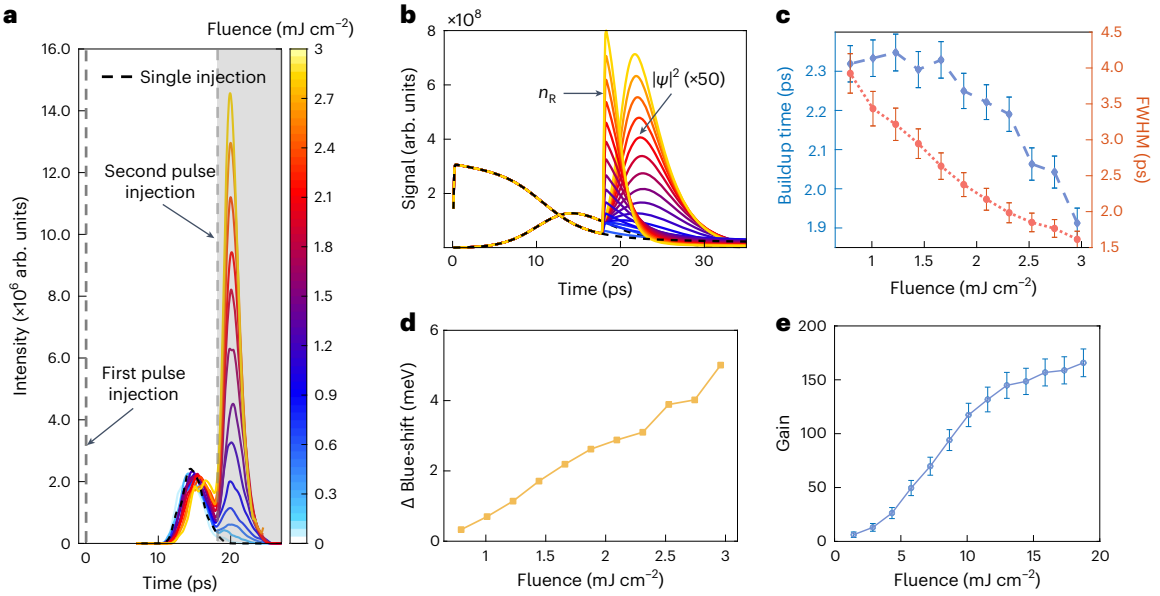

Fig. 4 | The dynamical amplification of the two-pulse non-resonant injection. The first injection pulse is fixed at ~1.5F_{th} above the condensation threshold. **a**, Time-resolved photoluminescence intensity obtained at various strengths for the second laser pulse. The dashed lines indicate the arrival times of the two injection laser pulses. **b**, The calculated dynamics of the exciton reservior (n_R) and the polaritons ($|\psi|^2$) for the experimental conditions in **a**. **c**, Fluence-dependent buildup time and bandwidth. Data are presented as mean values ± s.e.m. (n = 3). **d**,**e**, Energy shift (**d**) and signal gain (**e**) (defined as the ratio of the integrated signal in the grey region in **a** to that without a second pulse injection). Data are presented as mean values ± s.e.m. (n = 3).

Polariton temporal OR gate based on amplification

Now we turn to the scenario in which the fluence of the first pumping pulse is above the condensation threshold. Here, an initial EP condensate is produced by the first pulsed injection into the microcavity. In this situation, sudden stimulated bosonic amplification can be induced by the second pumping pulse injected at exactly the same location due to the past existence of a polariton population. The successive injection causes a fast population gain as long as the arrival time of the second pulse is in the presence of the condensate. The gain builds up in a shorter time compared with the situation in which the two injection pulses are below condensation threshold.

The actual gain is determined by the injection fluence of the second laser pulse, as shown in Fig. 4. Here the injection strength of the first pulse is fixed at ~1.5F_{th}, and the second pump pulse arrives at a time delay of about 17 ps. As can be seen in Fig. 4a, the amplification is stronger for a higher fluence of the second coming laser pulse. The behaviour is well-reproduced in our simulations, as shown in Fig. 4b. The corresponding buildup time (defined as the time from the second pulse injection to the peak of the amplification signal) for the enhancement and the width (FWHM) for the enhanced signal peak are extracted and shown in Fig. 4c. This amplification behaviour shows a transient response, which presents a very short buildup time of about 2 ps. As the fluence of the second pulse is increased from about 0.1F_{th} to F_{th}, the signal gain growing with the buildup time decreases by about 400 fs. The FWHM (indicated in Fig. 4c) of the amplified condensate decreases from approximately 3.9 ps to 1.6 ps, accompanied by an energy blue-shift of up to about 5 meV (Fig. 4d). Due to an increased degree of polariton replenishment, the enhanced interaction in the quasi-particle ensemble accelerates the condensation buildup and decay process[40], inducing an energy blue-shift. The gain (defined as the ratio of the integrated intensity in the grey and the white regions in Fig. 4a) increases as the strength of the second pulse increases. In Fig. 4e we can see that the fluence-dependent gain shows a linearly increasing region and a saturating region for second injection fluences beyond 1.2 mJ cm^{-2}. The maximum gain obtained in this measurement is about 12.5 dB.

On the basis of the above, a polariton temporal OR gate can be operated by increasing the input signal level such that either one is above the condensation threshold ($P_A > P_{th}$ or $P_B > P_{th}$). In this scenario, the table of the OR gate in Fig. 1 can be satisfied. All three kinds of logical gate functions can be realized by precisely controlling the strength of, and the relative delay between, the two injection pulses.

Discussion

Before this work, polariton logical gates were realized by cascading several spatially separated polaritonic transistors, where the output of one transistor is propagated towards a different location that is to be used as the input of a second transistor. Compared with such spatially defined transistors, our scheme, which is based on temporal polariton logic gates, exhibits the following features. First, this is a novel scheme in EP systems such that information is encoded and processed in the temporal domain by taking advantage of the non-equilibrium nature of the strongly coupled excitons and photons. Without spatial flow of the quasiparticles, both the room-temperature and localized operation guarantee a fast response time. For instance, we have achieved a 80 fs response time for the polariton temporal NOT gate. Moreover, such an information capacity only occupies a single dimension, that is, the temporal degree of freedom. The capacity can be largely extended by combining the manipulations with extra degrees of freedom. Second, the cascaded operation in the time domain requires a relatively simpler set-up. In our scheme, only two non-resonant laser pulses with controlled time delays are required as the 'inputs' for the polariton temporal logic gates. The cascaded polariton transistors are activated at the same location, and the final output signal can be obtained with a time-resolved detection in the transmission geometry. In comparison, three beams of spatially separated lasers—with various incident angles and energies—are usually needed to operate polaritonic transistors in a cascaded geometry based on spatially flowing polaritons[26,29]. Third, the complication to confine the polariton fluid in a microcavity, required by the realization of cascadability of multi-stage polariton transistors, can be removed with the current temporal logical gate scheme. The dependence of the device functionality on the quality of the microcavity can be greatly reduced. Overall, our temporally based polariton logical

gates show robustness, universality and ultrafast operation. Combined with polaritonic structures in spatial dimensions, the information processing capability can be dramatically enhanced, opening new horizons for implementing polariton integrated circuits.

Online content

Any methods, additional references, Nature Portfolio reporting summaries, source data, extended data, supplementary information, acknowledgements, peer review information; details of author contributions and competing interests; and statements of data and code availability are available at https://doi.org/10.1038/s41566-024-01483-2.

References

1. Khonina, S. N., Kazanskiy, N. L., Butt, M. A. & Karpeev, S. V. Optical multiplexing techniques and their marriage for on-chip and optical fiber communication: a review. *Opto-Electron. Adv.* **5**, 210127 (2022).
2. Smith, D. R. *Digital Transmission Systems* 177–257 (Springer, 2004).
3. Ansari, V., Donohue, J. M., Brecht, B. & Silberhorn, C. Tailoring nonlinear processes for quantum optics with pulsed temporal-mode encodings. *Optica* **5**, 534–550 (2018).
4. Richardson, D. J., Fini, J. M. & Nelson, L. E. Space-division multiplexing in optical fibres. *Nat. Photon.* **7**, 354–362 (2013).
5. Bergano, N. S. & Davidson, C. R. Wavelength division multiplexing in long-haul transmission systems. *J. Lightwave Technol.* **14**, 1299 (1996).
6. Chen, Z.-Y. et al. Use of polarization freedom beyond polarization-division multiplexing to support high-speed and spectral-efficient data transmission. *Light Sci. Appl.* **6**, e16207 (2016).
7. Yan, Y. et al. High-capacity millimetre-wave communications with orbital angular momentum multiplexing. *Nat. Commun.* **5**, 4876 (2014).
8. Lee, D., Sasaki, H., Fukumoto, H., Hiraga, K. & Nakagawa, T. Orbital angular momentum (OAM) multiplexing: an enabler of a new era of wireless communications. *IEICE Trans. Commun.* **E100.B**, 1044 (2017).
9. Dragoman, M. & Dragoman, D. *Advanced Optoelectronic Devices* Vol. 1 (Springer, 2013).
10. Hopfield, J. J. Theory of the contribution of excitons to the complex dielectric constant of crystals. *Phys. Rev.* **112**, 1555 (1958).
11. Weisbuch, C., Nishioka, M., Ishikawa, A. & Arakawa, Y. Observation of the coupled exciton–photon mode splitting in a semiconductor quantum microcavity. *Phys. Rev. Lett.* **69**, 3314 (1992).
12. Byrnes, T., Kim, N. Y. & Yamamoto, Y. Exciton–polariton condensates. *Nat. Phys.* **10**, 803–813 (2014).
13. Kasprzak, J. et al. Bose–Einstein condensation of exciton polaritons. *Nature* **443**, 409–414 (2006).
14. Balili, R., Hartwell, V., Snoke, D., Pfeiffer, L. & West, K. Bose–Einstein condensation of microcavity polaritons in a trap. *Science* **316**, 1007–1010 (2007).
15. Deng, H., Haug, H. & Yamamoto, Y. Exciton–polariton Bose–Einstein condensation. *Rev. Mod. Phys.* **82**, 1489 (2010).
16. Sanvitto, D. & Kéna-Cohen, S. The road towards polaritonic devices. *Nat. Mater.* **15**, 1061–1073 (2016).
17. Kavokin, A. et al. Polariton condensates for classical and quantum computing. *Nat. Rev. Phys.* **4**, 435–451 (2022).
18. Tsintzos, S. I., Pelekanos, N. T., Konstantinidis, G., Hatzopoulos, Z. & Savvidis, P. G. A GaAs polariton light-emitting diode operating near room temperature. *Nature* **453**, 372–375 (2008).
19. Christopoulos, S. et al. Room-temperature polariton lasing in semiconductor microcavities. *Phys. Rev. Lett.* **98**, 126405 (2007).
20. Antón, C. et al. Dynamics of a polariton condensate transistor switch. *Appl. Phys. Lett.* **101**, 261116 (2012).
21. Feng, J. et al. All-optical switching based on interacting exciton polaritons in self-assembled perovskite microwires. *Sci. Adv.* **7**, eabj6627 (2021).
22. Chen, F. et al. Optically controlled femtosecond polariton switch at room temperature. *Phys. Rev. Lett.* **129**, 057402 (2022).
23. Amo, A. et al. Exciton–polariton spin switches. *Nat. Photon.* **4**, 361–366 (2010).
24. Marsault, F. et al. Realization of an all optical exciton–polariton router. *Appl. Phys. Lett.* **107**, 201115 (2015).
25. Flayac, H. & Savenko, I. G. An exciton–polariton mediated all-optical router. *Appl. Phys. Lett.* **103**, 201105 (2013).
26. Ballarini, D. et al. All-optical polariton transistor. *Nat. Commun.* **4**, 1778 (2013).
27. Gao, T. et al. Polariton condensate transistor switch. *Phys. Rev. B* **85**, 235102 (2012).
28. Antón, C. et al. Quantum reflections and shunting of polariton condensate wave trains: implementation of a logic AND gate. *Phys. Rev. B* **88**, 245307 (2013).
29. Zasedatelev, A. V. et al. A room-temperature organic polariton transistor. *Nat. Photon.* **13**, 378 (2019).
30. Suchomel, H. et al. Prototype of a bistable polariton field-effect transistor switch. *Sci. Rep.* **7**, 5114 (2017).
31. Liew, T. C. H. et al. Proposal for a bosonic cascade laser. *Phys. Rev. Lett.* **110**, 047402 (2013).
32. Liew, T. C. H. et al. Quantum statistics of bosonic cascades. *New J. Phys.* **18**, 023041 (2016).
33. Sun, L. et al. Direct observation of whispering gallery mode polaritons and their dispersion in a ZnO tapered microcavity. *Phys. Rev. Lett.* **100**, 156403 (2008).
34. Chen, F. et al. Femtosecond dynamics of a polariton bosonic cascade at room temperature. *Nano Lett.* **22**, 2023 (2022).
35. Rutckaia, V. & Schilling, J. Ultrafast low-energy all-optical switching. *Nat. Photon.* **14**, 4–6 (2020).
36. Chen, F. et al. Ultrafast dynamics of exciton–polariton in optically tailored potential landscapes at room temperature. *J. Phys. Condens. Matter* **34**, 024001 (2021).
37. Chen, F. et al. Buildup dynamics of room-temperature polariton condensation. *Phys. Rev. B* **106**, L020301 (2022).
38. Xie, W. et al. Room-temperature polariton parametric scattering driven by a one-dimensional polariton condensate. *Phys. Rev. Lett.* **108**, 166401 (2012).
39. Zhang, X. H. et al. Exciton radiative lifetime in ZnO nanorods fabricated by vapor phase transport method. *Appl. Phys. Lett.* **90**, 013107 (2007).
40. Nardin, G. et al. Dynamics of long-range ordering in an exciton–polariton condensate. *Phys. Rev. Lett.* **103**, 256402 (2009).

Methods

Sample and experimental set-up

The ZnO microwire with regular hexagonal cross-section was fabricated by chemical vapour deposition method in a quartz furnace, forming a high-quality whispering gallery microcavity with a radius of about 1.8 μm and a quality factor of above 1,000. Due to the large exciton binding energy and strong oscillator strength, we can achieve strong coupling of excitons and cavity photons—and even bosonic condensation—in the ZnO microcavity at room temperature.

Ultrashort laser pulses with pulse durations of about 70 fs at the central wavelength of 350 nm were used to non-resonantly excite the quasiparticles at normal incidence in the ZnO microcavity. Two laser pulse beams were used as the driving pulses. The relative time delay of the two pulses was well-controlled by a high-precision motorized stage. Due to the different physical processes, various excitation parameters—such as pumping fluences and relative time delay—are required (see main text). The FARSI technique was used to capture the photoluminescence emission in the transmission direction in both the energy and momentum degrees of freedom with femtosecond resolution[34]. In this FARSI technique, photoluminescence emission was measured using angle-resolved spectroscopy in the Fourier plane, based on a 4*f* system[36], where a transient Kerr gating, driven by a beam of 35 fs pulses at 800 nm, was applied to the photoluminescence propagation path to obtain a time resolution of about 50 fs. The dispersions of all of the related optical elements in the set-up have been carefully calibrated and the absolute zero time has been precisely determined[22]. See the Supplementary Information for more details.

Simulation on the basis of the Gross–Pitaevskii equation

To clarify the dynamics of the non-equilibrium EP systems, an open-dissipative Gross–Pitaevskii equation coupled to an incoherent exciton reservoir is used to model the underlying processes[41,42]. In the simulation, the pump laser excites the system non-resonantly at a higher energy and creates an incoherent population of excitons, that is, reservoir excitons (n_R). They are strongly coupled with the cavity photons to produce EPs, which finally accumulate largely on the ground state to form a condensate at beyond the threshold density. The pump pulses are described by two Gaussian functions with a time delay τ. The second pulse can increase the population of the decaying exciton reservoir. The subsequent polariton density can be replenished with an extra injection, thus achieving the condensation threshold. The equations can be written as

$$P(\mathrm{t}) = P_1 \exp\left(-t^2/2\sigma^2\right) + P_2 \exp\left(-(t-\tau)^2/2\sigma^2\right) \quad (1)$$

$$\frac{\partial n_\mathrm{R}}{\partial \mathrm{t}} = P(t) + Rn_\mathrm{R}|\psi|^2 - \gamma_\mathrm{R} n_\mathrm{R} \quad (2)$$

$$i\frac{\partial \psi}{\partial t} = -\frac{\hbar}{2m}\nabla^2\psi + g_\mathrm{R} n_\mathrm{R}\psi + g_\mathrm{c}|\psi|^2 + i(Rn_\mathrm{R} - \gamma_\mathrm{c})\psi \quad (3)$$

Here $P(t)$ is the pump laser; R is the reservoir-condensate scattering rate; γ_R and γ_c are the decay rates of the excitons and the LPs, respectively; ψ is the wave function of the lower polariton mode; m is the effective mass of a polariton; and g_c and g_R represent the mean-field polariton–polariton and polariton–reservoir interaction constants, respectively.

Data availability

The data that support the findings of this study are available in the article and its Supplementary Information. Any additional information can be obtained from the corresponding authors on reasonable request. Source Data are provided with this paper.

References

41. Wouters, M. & Carusotto, I. Excitations in a nonequilibrium Bose–Einstein condensate of exciton polaritons. *Phys. Rev. Lett.* **99**, 140402 (2007).
42. Byrnes, T., Horikiri, T., Ishida, N., Fraser, M. & Yamamoto, Y. Negative Bogoliubov dispersion in exciton–polariton condensates. *Phys. Rev. B* **85**, 075130 (2012).

Acknowledgements

This work is supported by the National Natural Science Foundation of China (grant nos. 92250301, 12227807, 92050105 and 91950201), the Science and Technology Commission of Shanghai Municipality, China (grant nos. 23JC1402000 and 22ZR1419700) and the Shanghai Pilot Program for Basic Research (grant no. TQ20240204). T.B. is supported by the National Natural Science Foundation of China (grant no. 62071301); the NYU-ECNU Institute of Physics at NYU Shanghai; the Shanghai Frontiers Science Center of Artificial Intelligence and Deep Learning; the Joint Physics Research Institute Challenge Grant; the Science and Technology Commission of Shanghai Municipality (grant nos. 19XD1423000 and 22ZR1444600); the NYU Shanghai Boost Fund; the China Foreign Experts Program (grant no. G2021013002L); the NYU Shanghai Major-Grants Seed Fund; Tamkeen, under the NYU Abu Dhabi Research Institute grant (grant no. CG008); and the SMEC Scientific Research Innovation Project (grant no. 2023ZKZD55).

Author contributions

J.W. and H.L. conceived the idea and initiated the study. H.L., F.C., H.J. and Z.Y. conducted the experimental work. F.C., H.Z., J.S. and T.B. performed numerical simulations. S.L. provided sample support. Z.S., Huailiang Xu and Hongxing Xu provided technical support. All authors contributed to the data analysis and writing of the paper.

Competing interests

The authors declare no competing interests.

Additional information

Supplementary information The online version contains supplementary material available at https://doi.org/10.1038/s41566-024-01483-2.

Correspondence and requests for materials should be addressed to Hui Li or Jian Wu.

Peer review information *Nature Photonics* thanks Alexey Kavokin and the other, anonymous, reviewer(s) for their contribution to the peer review of this work.

Terms and Conditions

Springer Nature journal content, brought to you courtesy of Springer Nature Customer Service Center GmbH (“Springer Nature”).
Springer Nature supports a reasonable amount of sharing of research papers by authors, subscribers and authorised users (“Users”), for small-scale personal, non-commercial use provided that all copyright, trade and service marks and other proprietary notices are maintained. By accessing, sharing, receiving or otherwise using the Springer Nature journal content you agree to these terms of use (“Terms”). For these purposes, Springer Nature considers academic use (by researchers and students) to be non-commercial.
These Terms are supplementary and will apply in addition to any applicable website terms and conditions, a relevant site licence or a personal subscription. These Terms will prevail over any conflict or ambiguity with regards to the relevant terms, a site licence or a personal subscription (to the extent of the conflict or ambiguity only). For Creative Commons-licensed articles, the terms of the Creative Commons license used will apply.
We collect and use personal data to provide access to the Springer Nature journal content. We may also use these personal data internally within ResearchGate and Springer Nature and as agreed share it, in an anonymised way, for purposes of tracking, analysis and reporting. We will not otherwise disclose your personal data outside the ResearchGate or the Springer Nature group of companies unless we have your permission as detailed in the Privacy Policy.
While Users may use the Springer Nature journal content for small scale, personal non-commercial use, it is important to note that Users may not:

1. use such content for the purpose of providing other users with access on a regular or large scale basis or as a means to circumvent access control;
2. use such content where to do so would be considered a criminal or statutory offence in any jurisdiction, or gives rise to civil liability, or is otherwise unlawful;
3. falsely or misleadingly imply or suggest endorsement, approval , sponsorship, or association unless explicitly agreed to by Springer Nature in writing;
4. use bots or other automated methods to access the content or redirect messages
5. override any security feature or exclusionary protocol; or
6. share the content in order to create substitute for Springer Nature products or services or a systematic database of Springer Nature journal content.

In line with the restriction against commercial use, Springer Nature does not permit the creation of a product or service that creates revenue, royalties, rent or income from our content or its inclusion as part of a paid for service or for other commercial gain. Springer Nature journal content cannot be used for inter-library loans and librarians may not upload Springer Nature journal content on a large scale into their, or any other, institutional repository.
These terms of use are reviewed regularly and may be amended at any time. Springer Nature is not obligated to publish any information or content on this website and may remove it or features or functionality at our sole discretion, at any time with or without notice. Springer Nature may revoke this licence to you at any time and remove access to any copies of the Springer Nature journal content which have been saved.
To the fullest extent permitted by law, Springer Nature makes no warranties, representations or guarantees to Users, either express or implied with respect to the Springer nature journal content and all parties disclaim and waive any implied warranties or warranties imposed by law, including merchantability or fitness for any particular purpose.
Please note that these rights do not automatically extend to content, data or other material published by Springer Nature that may be licensed from third parties.
If you would like to use or distribute our Springer Nature journal content to a wider audience or on a regular basis or in any other manner not expressly permitted by these Terms, please contact Springer Nature at

onlineservice@springernature.com